

hp-ADAPTIVE EXTENDED FINITE ELEMENT METHOD

ANDREAS BYFUT AND ANDREAS SCHRÖDER

ABSTRACT. This paper discusses higher-order extended finite element methods obtained from the combination of the standard extended finite element method (XFEM) with higher-order finite element methods. Here, the focus is on the embedding of the latter into the partition of unity method, which is the basis of the XFEM. A priori error estimates are discussed and numerical verification is given for two benchmark problems. Moreover, methodological aspects are summarized which are necessary for *hp*-adaptivity in XFEM and allow for exponential convergence rates. In particular, the handling of hanging nodes via constraint approximation and an *hp*-adaptive strategy are presented.

1. INTRODUCTION

The extended finite element method (XFEM) is a widely studied approach for the modelling of cracks in linear elastic fracture mechanics. It is based on the partition of unity method (PUM) contrived by I. Babuška and J.M. Melenk in [8]. The development of the PUM was motivated by the need for new techniques for the solution of problems where the classical FEM fails or is prohibitively expensive. In the PUM a global conforming finite element space is constructed from a continuous partition of unity and a set of local approximation spaces which are supposed to approximate the sought solution well. The separation of the issues of inter-element continuity involved by the finite element method and the local approximability allows to focus on the retrieval of good local approximation spaces for a given problem. In the framework of linear elasticity and linear elastic fracture mechanics, i.e., for the modeling of cracks, these local approximation spaces are chosen such that they are able to approximate the discontinuities due to crack paths and in particular the singularity due to crack tips well. The resulting approach – the XFEM – was originally proposed by T. Belytschko and T. Black in [16] and improved by T. Belytschko, J. Dolbow and N. Moës in [33, 51]. Ever since, there have been many contributions to the XFEM, see [1, 40, 62] for an overview.

In the XFEM approach, singularities arising from crack tips are directly embedded in the ansatz space. Therefore, if no other sources for singularities occur, the standard finite element discretization has to approximate only contributions that exhibit high regularity. At present, only lower-order finite elements and uniform mesh refinements (*h*-method) are applied to reduce the approximation error of the XFEM. This solely leads to algebraic convergence rates of lower-order. Then again, the high regularity assumptions admit the use of higher-order polynomials and, in particular, of the *p*-method on a fixed mesh with increasing polynomial degree. This makes algebraic rates of higher-order and even exponential convergence rates possible. Only few of the current publications on XFEM focus on higher-order. E.V. Iarve [47] and F.L. Stazi et al. [63] basically discuss the modeling of curved interfaces/cracks using higher-order shape functions. In P. Laborde et al. [49], various enhancements for the XFEM are proposed and their influence on the convergence properties are studied. Particularly, this is the first publication where optimal algebraic convergence rates are reported for the standard mode I/II benchmark problems using a higher-order XFEM with fixed polynomial degree $p \leq 3$

Date: November 22, 2010.

2000 Mathematics Subject Classification. 65N30, 74S05.

Key words and phrases. XFEM, GFEM, PUM, higher-order, *hp*-adaptivity, *hp*-strategy, hanging nodes, constraint approximation, linear elasticity.

and uniform mesh refinement. So far, higher-order approaches with $p > 3$ in the context of h - or p -method are not reported in the literature.

Considering general linear elastic problems defined on arbitrary domains, e.g., with reentrant corners, in the scope of the standard FEM, it is well-known that uniform mesh refinement is insufficient to obtain optimal algebraic convergence rates. Also, the exponential convergence of the p -method is lost in the presence of reentrant corners. Indeed, using adaptive mesh refinements (h -adaptivity) optimal algebraic rates can be recovered for most problems and even exponential rates are possible if varying polynomial degrees are adopted (hp -adaptivity).

In this paper, the XFEM and standard higher-order FEM are combined and discussed in terms of the PUM to obtain a higher-order XFEM. Using one-dimensional Lagrange-type and hierarchical shape functions in combination with tensor products, a partition of unity and suitable higher-order enrichment sets are defined. Given the partition of unity, the local enrichment sets for the modeling of cracks are introduced using the notation as given by I. Babuška and J.M. Melenk in [8]. Moreover, an assortment of essential methodological aspects for h - and hp -adaptivity in XFEM are presented.

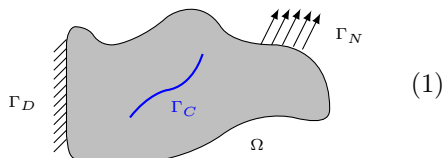
To define an adaptive scheme with automatic mesh refinement based on error control, suitable refinement strategies are needed to detect mesh elements to be refined and, additionally, elements whose polynomial degree has to be increased in h - and hp -adaptivity, respectively. In this paper, some basic h -adaptive strategies and a specific hp -adaptive strategy based on the estimation of local regularity are presented. Using local refinement of mesh elements, hanging nodes resulting from the refinement of mesh elements without the refinement of adjacent elements are generally inevitable devoid of sophisticated refinement strategies. For conform finite element schemes, the continuity of the finite element solution has to be ensured, e.g., by the constraint of degrees of freedom associated to hanging nodes. Using tensor product shape functions this can be done by constraint approximation which is also presented in this work. Finally, integration methods for higher-order XFEM are summarized.

Numerical experiments show that optimal algebraic and even exponential convergence rates are obtainable in the extended finite element method. A standard mode I benchmark problem with known solution is considered to show the desired rates for the h - and p -method. Also the combination of the higher-order XFEM with h - and hp -adaptivity is discussed through the study of a domain with reentrant corners. As an essential result of this paper, optimal algebraic and exponential convergence rates are obtained.

This paper is structured as follows: Section 2 commemorates the variational formulation and its discretization for a linear elastic model problem. In Section 3, the embedding of the XFEM into the PUM is discussed with focus on higher-order methods. The following Sections 4 and 5 define the partition of unity as well as some (higher-order) approximation sets via Lagrange-type and hierarchical shape functions, respectively. Sections 6 and 7 discuss some approximability results and methodological aspects for the higher-order XFEM. In Section 8 numerical results are presented. Section 9 concludes this paper.

2. PRELIMINARIES

Consider the boundary value problem to find a displacement field $\tilde{u} \in H^1(\Omega \setminus \Gamma_C; \mathbb{R}^2)$ in the presence of a (not necessarily traction-free) crack $\Gamma_C \subset \Omega$, that satisfies



$$\begin{aligned} \operatorname{div} \sigma(\tilde{u}) + f &= 0 & \text{in } \Omega, \\ \tilde{u} &= u_D & \text{on } \Gamma_D, \\ \sigma(\tilde{u}) \cdot n &= g & \text{on } \Gamma_N, \\ \sigma(\tilde{u}) \cdot n &= g & \text{on } \Gamma_C, \end{aligned}$$

where Ω is an open subset of \mathbb{R}^2 . Furthermore, $\sigma(\tilde{u}) = \mathbb{C} \varepsilon(\tilde{u}) = \lambda \operatorname{tr} \varepsilon(\tilde{u}) I + 2\mu \varepsilon(\tilde{u})$ is the

Cauchy stress tensor, \mathbb{C} is the fourth-order material tensor in generalization of Hooke's law, λ , μ are the Lamé constants and $\varepsilon(\tilde{u}) = \frac{1}{2}(\nabla\tilde{u} + \nabla\tilde{u}^T)$ is the linearized Green strain tensor. Moreover, assume that $f \in L^2(\Omega \setminus \Gamma_C; \mathbb{R}^2)$, $u_D \in H^1(\Omega \setminus \Gamma_C; \mathbb{R}^2)$ and $g \in L^2(\Gamma_N \cup \Gamma_C; \mathbb{R}^2)$, where L^2 , H^1 denote the usual Lebesgue and Sobolev spaces, respectively.

Given $\tilde{u} = u + u_D$, the variational formulation for the boundary value problem above is to find $u \in \mathcal{V} := H_D^1(\Omega \setminus \Gamma_C; \mathbb{R}^2) := \{v \in H^1(\Omega \setminus \Gamma_C; \mathbb{R}^2) \mid \gamma(u) = 0 \text{ on } \Gamma_D\}$ with trace operator γ , such that

$$(2) \quad a(u, v) = b(v) - a(u_D, v)$$

for all $v \in \mathcal{V}$ with

$$a(u, v) := \int_{\Omega} \sigma(u) : \varepsilon(v) \, dx,$$

$$b(v) := \int_{\Omega} f \cdot v \, dx + \int_{\Gamma_N \cup \Gamma_C} g \cdot \gamma(v) \, ds.$$

The existence of a unique solution to this variational problem is a consequence of Korn's inequality and the Lax Milgram Lemma, cf. [26].

In order to find an approximation u_h of u , the space \mathcal{V} is replaced by some finite dimensional space $\mathcal{V}_h \subset \mathcal{V}$. Hence, the discretized version of the variational problem (2) is to find $u_h \in \mathcal{V}_h$ such that

$$(3) \quad a(u_h, v_h) = b(v_h) - a(u_D, v_h)$$

for all $v_h \in \mathcal{V}_h$. Given some basis $\{\eta_k\}$ of \mathcal{V}_h , the approximation u_h is given by

$$u_h = \sum_k x_k \eta_k,$$

where x is the solution vector of the linear system of equations $Ax = d$ for the stiffness matrix A with $A_{k\ell} := a(\eta_k, \eta_\ell)$ and the load vector d with $d_k = b(\eta_k) - a(u_D, \eta_k)$. The following sections discuss the construction of an appropriate basis $\{\eta_k\}$ for the definition of a higher-order finite dimensional space \mathcal{V}_h based on the Partition of Unity Method.

3. HIGHER-ORDER EXTENDED FINITE ELEMENT METHOD — A PARTITION OF UNITY METHOD

In accordance with the partition of unity method (PUM) as proposed in [8], let $\{\Omega_i\}_{i \in \mathcal{M}}$ be an open cover of $\Omega \subset \mathbb{R}^2$ such that there exists a constant $M \in \mathbb{N}$ satisfying the overlap condition

$$(4) \quad \text{card}\{i : x \in \Omega_i\} \leq M$$

for all $x \in \Omega$. Furthermore, let $\{\varphi_i\}_{i \in \mathcal{M}}$ be a Lipschitz continuous partition of unity subordinate to $\{\Omega_i\}_{i \in \mathcal{M}}$ with $\sum_{i \in \mathcal{M}} \varphi_i \equiv 1$ on Ω , as well as

$$(5) \quad \text{supp } \varphi_i \subset \bar{\Omega}_i, \quad \|\varphi_i\|_{L^\infty(\mathbb{R}^2)} \leq C_\infty, \quad \|\nabla \varphi_i\|_{L^\infty(\mathbb{R}^2)} \leq \frac{C_G}{\text{diam } \Omega_i}$$

for all $i \in \mathcal{M}$ and some constants $C_G, C_\infty \in \mathbb{R}$. Here, L^∞ denotes the Lebesgue space of measurable functions bounded in the usual essential supremum norm. Thus, a higher-order extended finite element space may be defined as

$$(6) \quad \mathcal{V}_h = \text{span}_k \eta_k := \text{span}_{\substack{i \in \mathcal{M}, \\ j \in \{0,1\}}} \{v \varphi_i e_j \mid v \in V_i\} \subset \mathcal{V}$$

for the standard Euclidian basis $\{e_j\}_{j \in \{0,1\}}$ of \mathbb{R}^2 and some local approximation sets $\{V_i\}_{i \in \mathcal{M}}$, to be defined below.

Following the usual enrichment strategy for the modeling of cracks in the XFEM, cf. [51], let $J \subset \mathcal{M}$ be the set of indices whose associated patches $\{\Omega_j\}_{j \in J}$ are entirely cut by the crack

Γ_C . Furthermore, let $K_0, K_1 \subset \mathcal{M}$ be the sets of indices whose associated patches are close to the two individual crack tips P_0, P_1 of Γ_C for some distance function $d : \mathbb{R}^2 \times \mathbb{R}^2 \rightarrow \mathbb{R}_0^+$, i.e.,

$$(7) \quad K_\ell := \{i \in \mathcal{M} \mid \exists x \in \Omega_i : d(x, P_\ell) \leq \delta\},$$

for some $\delta \in \mathbb{R}_0^+$ and $\ell = 0, 1$. Thus, the local approximation sets can be defined as

$$(8) \quad V_i := \begin{cases} V_i^R \cup V_i^H, & i \in J, \\ V_i^R \cup V_0^W, & i \in K_0, \\ V_i^R \cup V_1^W, & i \in K_1, \\ V_i^R, & \text{otherwise} \end{cases}$$

for some sets of higher-order polynomials V_i^R and

$$\begin{aligned} V_i^H &:= \{vH \mid v \in V_i^R, \text{supp } v \cap \Gamma_C \neq \emptyset\}, \\ V_0^W &:= \{-\chi_0(v \circ \Psi_0) \mid v \in W\}, \\ V_1^W &:= \{\chi_1(v \circ \Psi_1) \mid v \in W\}. \end{aligned}$$

Here, Ψ_0, Ψ_1 denote translations and/or rotations of the usual crack tip functions,

$$(9) \quad W := \left\{ \sqrt{r} \sin \frac{\theta}{2}, \sqrt{r} \cos \frac{\theta}{2}, \sqrt{r} \sin \frac{\theta}{2} \sin \theta, \sqrt{r} \cos \frac{\theta}{2} \sin \theta \right\},$$

to match the individual crack tips of Γ_C . Moreover, $\chi_\ell \in W^{2,\infty}(\mathbb{R}^2; [0, 1])$, $\ell = 0, 1$ are so-called cut-off or ramp functions satisfying

$$(10) \quad \chi_\ell(x) = \begin{cases} 1, & d(x, P_\ell) \leq r_0, \\ 0, & d(x, P_\ell) \geq r_1 \end{cases}$$

for some $r_0, r_1 \in \mathbb{R}_0^+$ with $r_0 < r_1$, see also [24, 25, 39, 49, 70, 73]. As usual in XFEM, the Heaviside function H is aligned with the crack Γ_C , so that it is capable of continuously modeling the possible displacement jump along the crack path in accordance with the crack tip functions. This may be achieved using the levelset method or the vector levelset method proposed in [64, 66] and [21, 72], respectively.

So far, the definition of the extended finite element space (6) is custom-tailored to match the linear elastic boundary value problem (1), but lacks an appropriate definition of the partition of unity functions φ_i and those sets of (higher-order) polynomials V_i^R for every patch Ω_i , $i \in \mathcal{M}$. To resolve this, the following Sections 4 and 5 will consider standard higher-order finite element methods based on Lagrange-type and hierarchical shape functions, respectively. In these methods, the shape functions for every element T of a quadrilateral-based mesh \mathcal{T} of Ω are defined via bijective mappings $\Phi_T : T_{\text{ref}} \rightarrow T \in \mathcal{T}$ of a set of shape functions ξ defined on a reference element $T_{\text{ref}} := [-1, 1]^2$. The set ξ yields a partition of unity as well as polynomial approximation sets on T_{ref} . Hence, the mapped sets $\xi \circ \Phi_T^{-1}$ yield *local* partitions of unity along with some *local* polynomial approximation sets for every T of \mathcal{T} . The usual ‘aggregation of matching’ shape functions thus generates a *global* partition of unity $\{\varphi_i\}$ along with some polynomial approximation sets $\{V_i^R\}$. The bijective mappings used for the transformation from the reference element may for instance be given by the polynomial

$$(11) \quad \Phi_T(\hat{x}_0, \hat{x}_1) := \frac{1}{4} \left((1 - \hat{x}_0)(1 - \hat{x}_1) P_{T,0} + (1 + \hat{x}_0)(1 - \hat{x}_1) P_{T,1} + (1 + \hat{x}_0)(1 + \hat{x}_1) P_{T,2} + (1 - \hat{x}_0)(1 + \hat{x}_1) P_{T,3} \right)$$

for the vertices $P_{T,j}$ of T in anti-clockwise order, as depicted in Figure 1.

Obviously, the definition of the partition of unity and the polynomial approximations sets may be done for standard higher-order shape functions defined on triangle-based meshes as well, see for instance [49]. However, this paper focuses on quadrilateral-based meshes as this

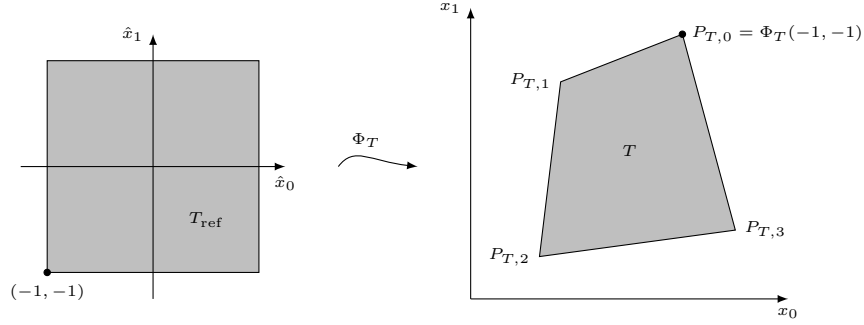


FIGURE 1. Bilinear mapping Φ_T from the reference element $T_{\text{ref}} = [-1, 1]^2$ to a element $T \in \mathcal{T}$.

allows for an easy definition of shape functions of ‘arbitrary’ polynomial degree employing tensor products.

4. LAGRANGE-TYPE SHAPE FUNCTIONS

In order to define the set of Lagrange-type shape functions ξ of partial degree p on T_{ref} , let $\{\hat{x}^0, \dots, \hat{x}^p\}$ be a set of unique supporting points defined on the interval $[-1, 1]$ with $\hat{x}^0 = -1$, $\hat{x}^p = 1$. Hence, the set of one-dimensional Lagrange-type shape functions $\{\hat{\xi}_i\}$ associated to $\{\hat{x}^i\}$ for $i \in \{0, \dots, p\}$ is given by

$$(12) \quad \hat{\xi}_i(\hat{x}) = \prod_{k=0, k \neq i}^p \frac{\hat{x} - \hat{x}^k}{\hat{x}^i - \hat{x}^k}.$$

Using $\hat{\xi}_i$, the set of two-dimensional tensor product Lagrange-type shape functions $\xi = \{\xi_\alpha\}$ defined on the reference element T_{ref} is given by

$$(13) \quad \xi_\alpha(\hat{x}_0, \hat{x}_1) = \hat{\xi}_{\alpha_0}(\hat{x}_0) \hat{\xi}_{\alpha_1}(\hat{x}_1)$$

for $\alpha \in \mathcal{A} := \{(\alpha_0, \alpha_1) \mid 0 \leq \alpha_r < p, r = 0, 1\}$. It is noted that the shape functions ξ_α and the supporting points $\hat{x}^\beta := (\hat{x}^{\beta_0}, \hat{x}^{\beta_1})$ are associated via the Kronecker delta property $\xi_\alpha(\hat{x}^\beta) = \delta_{\alpha\beta}$.

It is well-known that the set of Lagrange-type shape functions $\xi = \{\xi_\alpha\}_{\alpha \in \mathcal{A}}$ defined by (13) yields a higher-order partition of unity on the reference element T_{ref} . Using the bijective mappings (11), the mapped partition of unity functions $\xi_\alpha \circ \Phi_T^{-1}$ form local partitions of unity on every element T of the mesh \mathcal{T} . Let $\iota : \mathcal{A} \times \mathcal{T} \rightarrow \mathbb{N}$ associate a unique index to every mapped support point $\Phi_T(\hat{x}^\beta)$. The aggregation of all of these mapped local partition of unity functions associated to the same mapped supporting point, thus yields a global partition of unity $\{\varphi_i\}_{i \in \mathcal{M}}$ with $\mathcal{M} := \iota(\mathcal{A}, \mathcal{T})$ and $\Omega_i := \text{supp } \varphi_i$ via

$$(14) \quad \varphi_i|_T := \begin{cases} \xi_\alpha \circ \Phi_T^{-1} & i = \iota(\alpha, T), \\ 0 & \text{otherwise} \end{cases}$$

for $i \in \mathcal{M}$ and $T \in \mathcal{T}$. As there is no shape function left over from the definition of the partition of unity, the polynomial approximation sets are defined as $V_i^R \equiv \{1\}$.

Given the definition of the extended finite element space (6) via the Lagrange-type partition of unity functions (14), it is pointed out that all partition of unity functions φ_i with $i \in K_0 \cup K_1$ are enriched with the rotated/translated crack tip functions (9). This is depicted in Figure 2 for first- and third-order Lagrange-type partition of unity functions. In general, the distance δ used in (7) for the definition of K_0 and K_1 has to be chosen independently of the mesh density in order to achieve optimal convergence rates, see for instance Section 6 or [15, 49]. Obviously, if higher-order Lagrange-type partition of unity functions are chosen to improve

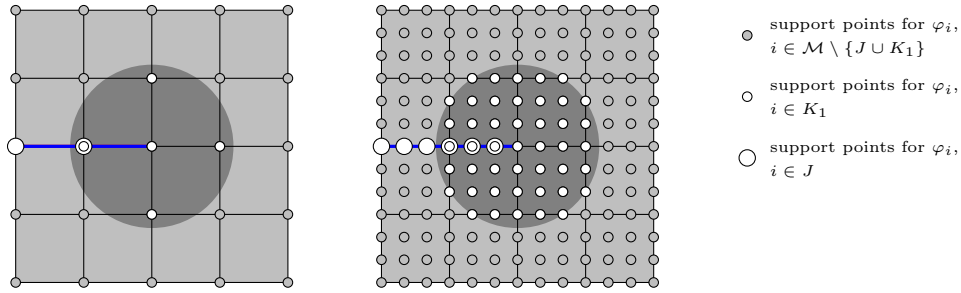


FIGURE 2. Visualization of enriched first- and third-order Lagrange-type partition of unity functions φ_i for a half-way horizontally cracked square-domain.

the overall convergence rate, then the number of partition of unity functions to be enriched with the crack tip functions increases drastically. Thus, computational cost is also drastically increased, in particular, due to the expensive integration of the crack tip functions. Even worse, for higher-order partition of unity functions, the condition numbers for the resulting linear systems of equations increase drastically too. The latter is due to the smooth nature of the crack tip functions away from the very crack tip and the high approximability of the higher-order partition of unity functions for smooth functions.

To ease the above mentioned problems and to stay within the framework of the partition of unity method, it is of advantage to have a partition of unity that is of lower-order in the vicinity of crack tips and of higher-order away from crack tips. However, using the Lagrange-type shape functions (13), it is difficult to handle elementwise anisotropic and, in particular, varying polynomial degrees, e.g., elements with lower polynomial degrees in the vicinity of crack tips and elements with higher polynomial degrees away from crack tips.

In order to evade the latter, it is suggested in [49, 63] to introduce additional first-order shape functions in the vicinity of crack tips to be used solely for the crack tip enrichments as depicted in Figure 3. However, this basically means that the concept of the partition of unity

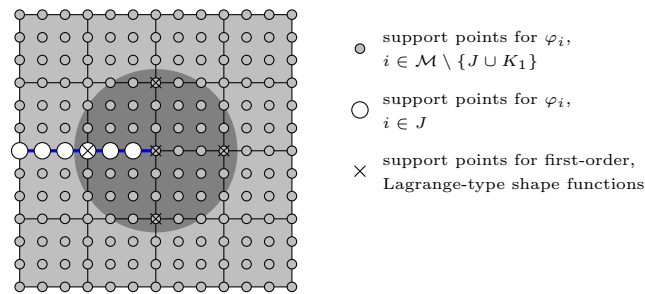


FIGURE 3. Visualization of enriched third-order Lagrange-type partition of unity functions φ_i and the additional first-order Lagrange-type shape functions for a half-way horizontally cracked square-domain.

method is left aside. Moreover, the convergence rates for this approach are clearly sub-optimal, cf. [49, Fig. 11]. Congruously, the solution proposed in [49] to achieve optimal convergence rates is given in the section “Back to the PUFEM”. The idea described therein (without the transition layer tending to zero) is basically the same as in [39], where a ‘ramp function’ is used to cancel ‘unwanted terms’ in the transition layer between crack tip enriched and non-enriched elements. It is noted that the definition of the higher-order extended finite element space (6) includes this ramp function technique for $\delta = r_1$ in (7) and (10).

An alternative to the introduction of additional lower-order shape functions as above, is the definition of a global lower-order partition of unity along with some higher-order polynomial enrichment functions. In the literature this technique is referred to as *p*-adaptivity in the generalized finite element method or as the *hp*-cloud method, see [13, 14] and [35, 55], respectively. But then, there are some standard higher-order finite element methods that basically do the very same. For instance, consider the following modified set of Lagrange-type shape functions

$$(15) \quad \hat{\xi}_0(\hat{x}) = \frac{1}{2}(1 - \hat{x}), \quad \hat{\xi}_p(\hat{x}) = \frac{1}{2}(1 + \hat{x}), \quad \hat{\xi}_i(\hat{x}) = \frac{\hat{\xi}_0(\hat{x})\hat{\xi}_p(\hat{x})}{\hat{\xi}_0(\hat{x}^i)\hat{\xi}_p(\hat{x}^i)} \prod_{k=1, k \neq i}^{p-1} \frac{\hat{x} - \hat{x}^k}{\hat{x}^i - \hat{x}^k}$$

for $i = 1, \dots, p-1$, where $\{\hat{x}^0, \dots, \hat{x}^p\}$ is a set of unique support points defined on $[-1, 1]$ with $\hat{x}^0 = -1$ and $\hat{x}^p = 1$, as proposed in [29]. The shape functions $\hat{\xi}_0, \hat{\xi}_p$ yield a linear partition of unity on $[-1, 1]$, where as the higher-order shape functions $\hat{\xi}_i, i = 1, \dots, p-1$ can obviously be factorized into either $\hat{\xi}_0$ or $\hat{\xi}_p$ and some remainder polynomials, which may serve as polynomial enrichment functions.

Given the Lagrange-type shape functions (15) or the ramp function technique, it is possible to define a higher-order extended finite element space \mathcal{V}_h of some fixed global polynomial degree. Then again, the intrinsic goal for all higher-order finite element methods is to obtain exponential convergence rates. For arbitrary domains with, for instance, reentrant corners, this remains unachievable as long as varying polynomial degrees cannot be modeled appropriately in the sense of *hp*-FEM. In standard *hp*-FEM, elementwise varying polynomial degrees are usually realized via hierarchical shape functions. The following section will discuss these shape functions in terms of the PUM, allowing for an appropriate definition of an *hp*-adaptive XFEM.

It is noted, that apart from their ability to easily allow for varying and, moreover, anisotropic polynomial degrees, these hierarchical shape functions have proven to be highly efficient in *hp*-FEM while significantly improving the condition number of the resulting linear system of equations compared to Lagrange-type shape functions, cf. [75]. Due to their tensor product structure and, in particular, their definition via a recurrence relation, these shape functions and their derivatives can be evaluated numerically stable.

5. HIERARCHICAL SHAPE FUNCTIONS

Similar to the modified set of Lagrange-type shape functions (15), the entire set of hierarchical shape functions does not yield a partition of unity for polynomial degrees $p > 1$. However, the subset of bilinear nodal modes of these shape functions does. The aim of this section is to formally define the polynomial enrichment sets $V_i^R, i \in \mathcal{M}$, such that $\varphi_i V_i^R, i \in \mathcal{M}$ generates the usual global hierarchical basis functions of the *p*-method along with their well-studied approximability properties. This definition is done in three steps: First, hierarchical shape functions based on integrated Legendre and Gauss-Lobatto polynomials are introduced and separated into nodal, edge and inner modes using a concise notation. Then, a simple data structure is proposed that is capable of handling the so-called edge orientation problem. Using a numbering based on that data structure, the sets of polynomials V_i^R are defined via an elementwise aggregation of suitably factorized edge and inner modes. A visualization of such an factorization is depicted in Figure 4. It is noted that the partition of unity and the polynomial enrichment sets V_i^R for the modified set of Lagrange-type shape functions (15) can be defined in the same fashion.

5.1. Hierarchical shape functions. A widely used family of hierarchical shape functions for higher-order FEM is generated by tensor products of integrated Legendre or Gauss-Lobatto polynomials, cf. [48, 61, 68]. Both types of polynomials are defined via the Gegenbauer

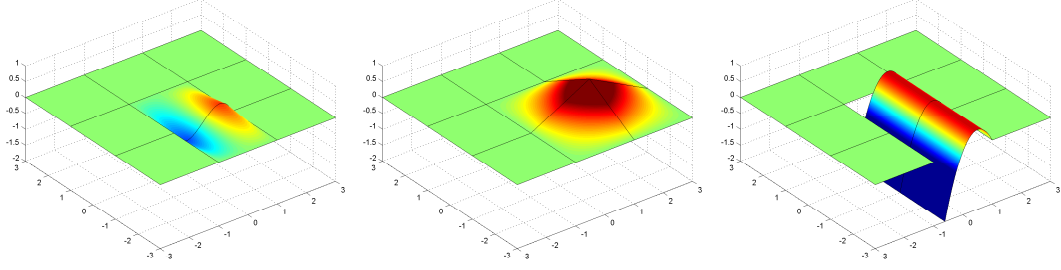


FIGURE 4. Visualization of the factorization of a third-order hierarchical shape function (left) into a bilinear partition of unity function (middle) and some elementwise quadratic remainder polynomial (right).

polynomials $\{G_i^\rho\}_{i \in \mathbb{N}_0}$ given by the recurrence relation

$$(16) \quad (i+1)G_{i+1}^\rho(\hat{x}) = 2(i+\rho)\hat{x}G_i^\rho(\hat{x}) - (i+2\rho-1)G_{i-1}^\rho(\hat{x})$$

with $G_0^\rho(\hat{x}) := 1$ and $G_1^\rho(\hat{x}) := 2\rho\hat{x}$ for $\rho \in \mathbb{R}$. The one-dimensional integrated Legendre shape functions ($\kappa_i \equiv 1$) and the Gauss-Lobatto shape functions ($\kappa_i = \sqrt{(2i-1)/2}$) up to a polynomial degree $p \geq 1$ are given by

$$(17) \quad \hat{\xi}_0(\hat{x}) := (1-\hat{x})/2, \quad \hat{\xi}_1(\hat{x}) := (1+\hat{x})/2, \quad \hat{\xi}_i(\hat{x}) := \kappa_i G_i^{-1/2}(\hat{x})$$

for $\hat{x} \in [-1, 1]$ and $i = 2, \dots, p$.

To define the set of two-dimensional Gegenbauer-type shape functions and to separate them into nodal, edge and inner modes with possibly varying maximal polynomial degrees, let $b = (b_0, b_1)$ be the 2-tuplet with values in \mathbb{N}_0 that is uniquely associated to each vertex, each edge and the unit quadrilateral itself, as depicted in Figure 5(a) with $p_0, \dots, p_5 \geq 2$. With these preparations at hand, the nodal, edge and inner modes associated to their individual 2-tuplet b are simply given by $\{\xi_\alpha\}_{\alpha \in \mathcal{A}(b)}$ with $\xi_\alpha(\hat{x}_0, \hat{x}_1) := \hat{\xi}_{\alpha_0}(\hat{x}_0)\hat{\xi}_{\alpha_1}(\hat{x}_1)$, where

$$\mathcal{A}(b) := \{\alpha = (\alpha_0, \alpha_1) \mid \alpha_r := b_r \text{ if } b_r \in \{0, 1\}, \text{ otherwise } \alpha_r \in \{2, \dots, b_r\}\}.$$

It is noted that $p_i \neq p_j$ results in anisotropic polynomial degree distributions. For $p_0 = p_1 = p_2 = p_3$ and $p_4 = p_5 = p_0 - 2$ Serendipity shape functions are generated, cf. [4, 68].

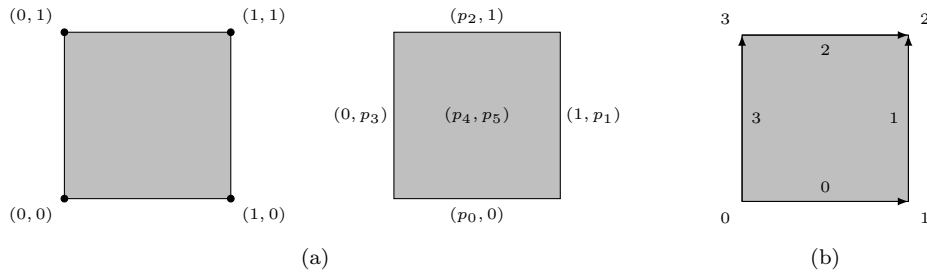


FIGURE 5. Index tuples identifying nodes, edges and the reference quadrilateral itself (a). Visualization of natural edge orientations (b).

5.2. A simple data structure and the orientation problem. In most finite element implementations, vertices, edges and elements of a decomposition \mathcal{T} of Ω are represented by a special data structure which enables the storage of information like coordinates, polynomial degrees and global numbering or allows for the generation of some information about its connectivity. For the definition of such a data structure, let an ℓ -node be defined as a vertex ($\ell = 0$), an edge ($\ell = 1$) or an element ($\ell = 2$) of \mathcal{T} . Furthermore, let $\mathcal{N}_\ell \subset \mathbb{N}$, $0 \leq \ell \leq 2$ be

sets of indices which uniquely identify all ℓ -nodes of \mathcal{T} and let $\tau : \mathcal{T} \rightarrow \mathcal{N}_2$ be a mapping that identifies an element with its associated element index. In order to be able to formally access the connectivity of each ℓ -node in \mathcal{N}_ℓ , let there be a mapping

$$N_r^\ell : \mathcal{N}_\ell \times \mathcal{Z}_r^\ell \rightarrow \mathcal{N}_r \quad \text{with} \quad \mathcal{Z}_r^\ell := \left\{0, \dots, \frac{2^{\ell-r} \ell!}{r! (\ell-r)!} - 1\right\},$$

which uniquely associates each ℓ -node with all of its adjacent r -nodes, $0 \leq r \leq \ell \leq 2$. In particular, $N_r^\ell(i, j)$ refers to the j -th adjacent r -node of the i -th ℓ -node and $N_\ell^\ell(i, 0)$ refers to the i -th ℓ -node itself. A data structure with similar naming has been proposed in [27, 30].

To ensure aggregated edge modes and their factorizations to be continuous over edges, it is of great importance to take the orientation of the edges into account. A natural local orientation of edges resulting from the definition of ξ via a tensor product is depicted in Figure 5(b). This orientation is equivalently given by

$$(18) \quad D := \begin{pmatrix} 0 & 1 & 3 & 0 \\ 1 & 2 & 2 & 3 \end{pmatrix},$$

where the entries of the j -th column denote the vertex indices of the edge with index j . For a consistent definition of edge and vertex indices for each element in \mathcal{N}_2 and of vertex indices for each edge in \mathcal{N}_1 in accordance with the natural orientation of edges (18), assume that for all $i \in \mathcal{N}_2$ and all $j \in \mathcal{Z}_1^2$, there exists a unique index $\nu_{ij} \in \mathcal{Z}_0^1$ such that

$$N_0^2(i, D_{rj}) = N_0^1(N_1^2(i, j), (r + \nu_{ij}) \bmod 2)$$

for all $r \in \mathcal{Z}_0^1$. This property is used to solve the so-called edge orientation problem implied by the natural orientation D . For two neighboring elements, the orientation of the common edge is generally not the same. To ensure continuity in the aggregation of edge modes associated to a common edge, define the mapping $h : \mathcal{N}_2 \times \mathcal{Z}_1^2 \rightarrow \{-1, 1\}$, $h(i, j) := 2\nu_{ij} - 1$. This mapping will be used in (20) for the definition of factorized and aggregated edge modes.

5.3. Construction of the partition of unity functions φ_i and the sets V_i^R . For the proper definition of a higher-order XFEM with varying and anisotropic polynomial degrees, assume some global degree distribution $\mathcal{P}_r : \mathcal{N}_r \rightarrow \mathbb{N}^r$ that assigns some polynomial degrees to each r -node in \mathcal{N}_r for $r \in \{1, 2\}$. Note that there are no polynomial degrees associated to 0-nodes, i.e. vertices, as their associated shape functions are bilinear by definition. Given this degree distribution, define a mapping $b_r : \mathcal{N}_2 \times \mathcal{Z}_r^2 \rightarrow \mathbb{N}^2$, $r = 0, 1, 2$ so that $b_r(i, j)$ is the 2-tuple associated to the j -th adjacent r -node of the i -th 2-node in \mathcal{N}_2 as depicted in Figure 5, so that $p_k := \mathcal{P}_1(N_1^2(i, k))$, $k = 0, \dots, 3$, and $(p_4, p_5) := \mathcal{P}_2(i)$. Furthermore, let $g_\ell : \mathcal{N}_\ell \times \mathcal{T} \rightarrow \mathcal{Z}_\ell^2 \cup \{-1\}$ for $\ell \in \{0, 1\}$ with $g_\ell(i, T) := j$ if there exists a $j \in \mathcal{Z}_\ell^2$ satisfying $i = N_\ell^\ell(\tau(T), j)$, and $g_\ell(i, T) := -1$ otherwise.

Considering the hierarchical shape functions defined in Subsection 5.1, it is easy to find that the nodal modes yield a partition of unity on the reference element T_{ref} , i.e.,

$$\sum_{\alpha \in \{0, 1\}^2} \xi_\alpha \equiv 1.$$

Consequently, these modes yield local partitions of unity on every element $T \in \mathcal{T}$, which can easily be merged to a global partition of unity $\{\varphi_i\}_{i \in \mathcal{M}}$ with $\mathcal{M} := \mathcal{N}_0$ and $\Omega_i := \text{supp } \varphi_i$ via

$$(19) \quad \varphi_i|_T := \begin{cases} \xi_\alpha \circ \Phi_T^{-1} & j := g_0(i, T) \neq -1, \alpha := b_0(\tau(T), j), \\ 0 & \text{otherwise} \end{cases}$$

for $i \in \mathcal{M}$ and $T \in \mathcal{T}$.

The basic idea for the definition of the sets V_i^R is to factorize the edge and inner modes by the partition of unity functions (19). Choosing the partition of unity function associated to

the first vertex of every edge for the factorization, the factorized edges modes for $s \in \mathcal{N}_1$ and $2 \leq p \leq \mathcal{P}_1(s)$ are defined as

$$(20) \quad e_{s,p}|_T := \begin{cases} h(\tau(T), j)^p \frac{\xi_\alpha}{\xi_\beta} \circ \Phi_T^{-1} & j := g_1(i, T) \neq -1, \alpha \in \mathcal{A}(b_1(\tau(T), j)), p = \max_r \alpha_r, \\ 0 & \text{otherwise,} \end{cases}$$

where $\beta := b_0(\tau(T), k)$ with $k \in \mathcal{Z}_0^2$ satisfying $N_0^2(\tau(T), k) = N_0^1(s, 0)$. It is noted that the factor $h(\tau(T), j)^p$ ensures the continuity of the factorized edge modes across the edge $N_1^2(\tau(T), j)$ as it solves the edge orientation problem for the hierarchical shape functions ξ . Choosing the partition of unity function associated to the first vertex of every element for the factorization, the factorized inner modes for $t \in \mathcal{N}_2$ and $\alpha \in \mathcal{A}(b_2(\tau(T), 0))$ are given by

$$(21) \quad f_{t,\alpha}|_T := \begin{cases} \frac{\xi_\alpha}{\xi_\beta} \circ \Phi_T^{-1} & \tau(T) = t, \\ 0 & \text{otherwise,} \end{cases}$$

where $\beta := b_0(\tau(T), 0)$. With these preparations at hand, the polynomial enrichment sets are defined as

$$(22) \quad V_i^R := \{e_{s,p} \mid s \in \mathcal{N}_1, i = N_0^1(s, 0), 2 \leq p \leq \mathcal{P}_1(s)\} \cup \{f_{t,\alpha} \mid t \in \mathcal{N}_2, i = N_0^2(t, 0), \alpha \in \mathcal{A}(\mathcal{P}_2(t))\} \cup \{1\}.$$

It is noted that the choice of the partition of unity function associated to the first vertex of an edge and the first vertex of an element for the factorization in (20) and (21) is arbitrary.

It remains to show that the factorized edge and inner modes under the polynomial mapping Φ_T are polynomials. First, consider the factorized edge modes (20). Obviously, there exist $r, \tilde{r} \in \{0, 1\}$, $r \neq \tilde{r}$ with $\alpha_r \geq 2$ and $\alpha_{\tilde{r}} = \beta_{\tilde{r}}$, so that

$$(23) \quad \frac{\xi_\alpha}{\xi_\beta}(x_0, x_1) = \frac{\xi_{\alpha_r}}{\xi_{\beta_r}}(x_r) = \kappa_{\alpha_r} \frac{G_{\alpha_r}^{-1/2}(x_r)}{\frac{1}{2}(1 \pm x_r)}.$$

By induction, it follows that $G_i^{-1/2}(x)/(1-x^2)$, $i \geq 2$, is a polynomial. Therefore, (23) is a polynomial which shows that the factorized edge modes are also polynomials under the mapping Φ_T . Now, consider the factorized inner modes as defined in (21). There holds

$$(24) \quad \frac{\xi_\alpha}{\xi_\beta}(x_0, x_1) = \kappa_{\alpha_0} \kappa_{\alpha_1} \frac{G_{\alpha_0}^{-1/2}(x_0)}{\frac{1}{2}(1 \pm x_0)} \frac{G_{\alpha_1}^{-1/2}(x_1)}{\frac{1}{2}(1 \pm x_1)}$$

Again, since $G_i^{-1/2}(x)/(1-x^2)$ is a polynomial, it follows that (24) is a polynomial as well and, therefore, the factorized inner modes are also polynomials under the mapping Φ_T .

6. REMARK ON THE APPROXIMABILITY OF THE HIGHER-ORDER XFEM SPACE \mathcal{V}_h

For the following discussion, let $u = u_0^W + u_1^W + \tilde{u}^R H + u^R$ be a decomposition of the solution of the variational problem (2), where $\tilde{u}^R, u^R \in H^k(\Omega; \mathbb{R}^2)$ with $\text{supp } \tilde{u}^R = \bigcup_{i \in J} \Omega_i$. Assuming that the crack tip functions (9) adequately model the displacement in the vicinity of the crack tips, it is reasonable to suppose

$$(25) \quad u_\ell^W|_{\omega_\ell} \in \text{span} \left\{ (v \circ \Psi_\ell) e_j \mid v \in W \right\}_{j \in \{0,1\}}$$

for $\omega_\ell := \bigcup_{i \in K_\ell} \Omega_i$, $\ell = 0, 1$ and

$$(26) \quad u_\ell^W|_{\Omega \setminus B_\varepsilon(P_\ell)} = \bar{u}^R H$$

for the individual crack tips P_0, P_1 of the crack and $\bar{u}^R \in H^k(\Omega; \mathbb{R}^2)$ as well as some $\varepsilon > 0$ with $B_\varepsilon(P_\ell) \subsetneq \omega_\ell$.

To quantify the approximability of the extended finite element space (6) using the approximability results of the PUM, i.e., using Theorem 1 in [8], it is necessary to find upper bounds for the approximation error for the local approximation sets V_i on every patch Ω_i , $i \in \mathcal{M}$.

Given the assumption (25), there holds $u_0^W, u_1^W \in \text{span } V_i$ for all $i \in K_0 \cup K_1 \subset \mathcal{M}$. In the general case, assuming appropriately shaped patches Ω_i and V_i^R to consist of appropriate polynomials of degree $p_i \geq 1$, there exist some interpolation polynomials $v_i^R, \tilde{v}_i^R \in V_i^R$, $\text{supp } \tilde{v}_i^R = \bigcup_{i \in J} \Omega_i$ so that $v_i := \tilde{v}_i^R H + v_i^R \in \text{span } V_i$ satisfies

$$(27) \quad \begin{aligned} \|u - v_i\|_{L^2(\Omega \cap \Omega_i)} &\lesssim h_i^{\mu_i} p_i^{-(k-1)}, \\ |u - v_i|_{H^1(\Omega \cap \Omega_i)} &\lesssim h_i^{\mu_i-1} p_i^{-(k-1)} \end{aligned}$$

for all $i \in \mathcal{M} \setminus \{K_0 \cup K_1\}$, where $h_i := \text{diam } \Omega_i$ and $\mu_i := \min\{k, p_i + 1\}$, cf. [9, 18, 59]. Hence, employing $v_h := \sum_{i \in \mathcal{M}} \varphi_i v_i$, the partition of unity property as well as (4) and (5), there holds

$$|u - v_h|_{H^1(\Omega)} \lesssim h^{\mu-1} p^{-(k-1)},$$

where $h := \max_{i \in \mathcal{M}} h_i$ and $p := \min_{i \in \mathcal{M}} p_i$, cf. [8]. Finally, the approximability for an extended finite element solution $u_h \in \mathcal{V}_h$ is given by the well-known Céa-Lemma,

$$(28) \quad |u - u_h|_{H^1(\Omega)} \lesssim h^{\mu-1} p^{-(k-1)}.$$

The catch in the approximation result (28) is, that it depends on the polynomial degree p_i for the sets V_i^R and that it does not account for the approximability of the partition of unity itself. Considering the definition of the extended finite element spaces \mathcal{V}_h via the standard set of Lagrange-type shape functions as discussed in Sections 4, there holds $p_i \equiv 0$. Consequently, the local approximation property (27) cannot be applied. For the modified set of Lagrange-type shape functions and the hierarchical shape functions, there holds $p_i \geq 1$ depending on the chosen polynomial degree distributions \mathcal{P}_r . However, the local approximation property (27) of the remainder polynomials (22) is unclear, as they are only defined elementwise on Ω_i . At best, there may hold $p = \min \mathcal{P}_r - 1$ as the approximability of the bilinear partition of unity itself is neglected in (28). Similar results were already given in Remark 4.2 in [5] and a forthcoming paper was promised therein to address the problem above.

For the time being, the following more specialized approximation result will do. Given the regularity assumption (26), the supports of u_0^W and u_1^W of the decomposition of u can be limited using the ramp functions χ_0 and χ_1 as introduced in Section 3. Hence, there exist some $\hat{u}^R, \check{u}^R \in H^k(\Omega; \mathbb{R}^2)$ with $\text{supp } \hat{u}^R = \bigcup_{i \in J} \Omega_i$, such that

$$u = \chi_0 u_0^W + \chi_1 u_1^W + \hat{u}^R H + \check{u}^R \in \mathcal{V}.$$

Let $K_0, K_1 \subset \mathcal{M}$ be defined as in (7) and (10) with $\delta := r_1$. Using elementwise polynomials $\hat{v}_h^R, \check{v}_h^R \in \text{span}_{i \in \mathcal{M}} \varphi_i V_i^R \subset C^0(\Omega; \mathbb{R}^2)$ of degree p with $\text{supp } \hat{v}_h^R = \bigcup_{i \in J} \Omega_i$, there holds

$$v_h := \chi_0 u_0^W + \chi_1 u_1^W + \hat{v}_h^R H + \check{v}_h^R \in \mathcal{V}_h,$$

so that

$$|u - v_h|_{H^1(\Omega)} \lesssim |\hat{u}^R - \hat{v}_h^R|_{H^1(\Omega)} + |\check{u}^R - \check{v}_h^R|_{H^1(\Omega)}.$$

For a quasi-uniform parallelogram mesh \mathcal{T} as well as a Lipschitz domain Ω , the hp finite element interpolation results given in [9, 18, 59] yield

$$|u - v_h|_{H^1(\Omega)} \lesssim h^{\mu-1} p^{-(k-1)},$$

where p is the polynomial degree of $\text{span } \varphi_i V_i^R$ for all $i \in \mathcal{M}$. The application of the Céa-Lemma yields the approximability result for an extended finite element solution of (3). It is noted that the use of the ramp functions χ_ℓ in the above approximation result implies that the radius for the crack tip enrichment should be chosen independently of the mesh density. For more interpolation results of the standard hp -FEM, the interested reader is referred to [6, 7, 11, 42, 43, 61].

7. METHODOLOGICAL ASPECTS

This section summarizes a couple of methodological aspects necessary to obtain the results presented in Section 8. In particular, well-acknowledged hp -adaptive refinement strategies are commemorated and the handling of hanging nodes is discussed. For a broader overview of the other subjects in this section as well as many other subjects not mentioned here at all, see for instance [1, 40, 62].

7.1. hp -adaptive strategies. In adaptive finite element methods, meshes are automatically refined and polynomial degrees are increased exclusively wherever some refinement indicator suggests to do so. The aim is to generate more effective meshes accompanied by smaller computational cost. In many practical examples, desired convergence properties can be shown by numerical experiments, i.e., optimal algebraic rates in h -adaptivity and exponential rates in hp -adaptivity. However, these properties are generally not guaranteed a priori.

Adaptive strategies are usually based on a reliable error estimate $\eta = \eta(u_h)$ satisfying

$$\|u - u_h\|_{H^1(\Omega)} \leq C\eta,$$

where C is a mesh-independent constant. An import assumption on the estimate η is its representation as a sum of local error contributions η_T computable for each element $T \in \mathcal{T}$,

$$\eta^2 = \sum_{T \in \mathcal{T}} \eta_T^2.$$

In h -adaptive methods, mesh-refinement is based upon the error contributions by the individual elements. Various criteria to select elements to be refined are proposed in the literature, cf. [12, 74]. Here, three well-known criteria are commemorated. When applying a *fixed fraction criterion*, a fixed fraction $\theta \in [0, 1]$ of all elements with the largest error contributions η_T to the total error η is refined. Using a *maximum criterion*, all elements with an error larger than a fixed fraction $\theta \in [0, 1]$ of the largest error associated to a single element are refined, i.e., all elements T that satisfy $\eta_T > \theta \max_{\tilde{T} \in \mathcal{T}} \eta_{\tilde{T}}$. For the *bulk criterion*, the set of elements $\tilde{\mathcal{T}}$ to be refined is given by the elements with the largest error contributions to the total error η such that $\sum_{T \in \tilde{\mathcal{T}}} \eta_T^2 > \theta \eta^2$ for some $\theta \in [0, 1]$.

Using hp -adaptivity, one has to decide which mesh elements have to be refined and additionally for which the polynomial degree has to be increased. There is a variety of strategies discussed in the literature, see for instance [3, 32, 50, 57]. Most of these strategies rely on the estimation of the local regularity of the sought solution. If this local regularity is ‘sufficient’, the polynomial degree is increased. Otherwise, the element is refined. The hp -strategy applied in this paper is based on the estimation of the local regularity by two finite element approximations on the same mesh but with different degree distributions, as proposed in [67]. For this purpose, let $\eta^2 = \sum_{T \in \mathcal{T}} \eta_T^2$ and $\tilde{\eta}^2 = \sum_{T \in \mathcal{T}} \tilde{\eta}_T^2$ be two error estimates corresponding to an initial, elementwise defined degree distribution $p = \{p_T \in \mathbb{N}\}$ and a second distribution $\tilde{p} = \{\tilde{p}_T \in \mathbb{N}\}$, respectively. Using the notation of Section 5, the polynomial degree distribution \mathcal{P}_r is then obtained via $\mathcal{P}_2(t) := (p_{\tau^{-1}(t)}, p_{\tau^{-1}(t)})$ for all element indices $t \in \mathcal{N}_2$. The polynomial degree for an edge $s \in \mathcal{N}_1$ can be defined applying the minimum rule $\mathcal{P}_1(s) := \min_{T \in \mathcal{T}_s} p_T$ or the maximum rule $\mathcal{P}_1(s) := \max_{T \in \mathcal{T}_s} p_T$, where $\mathcal{T}_s \subset \mathcal{T}$ is the set of all elements adjacent to s , i.e., $\mathcal{T}_s := \{T \in \mathcal{T} \mid g_1(s, T) \neq -1\}$.

The main idea for the regularity estimation is to assume that the local error contributions η_T and $\tilde{\eta}_T$ for $T \in \mathcal{T}$ are approximatively described by the well-known a priori estimates,

$$\eta_T \approx C_T p_T^{-\varrho_T+1}, \quad \tilde{\eta}_T \approx C_T \tilde{p}_T^{-\varrho_T+1}$$

with $\varrho_T > 0$, cf. [9]. Provided that $p_T \neq \tilde{p}_T$, ϱ_T can then be approximated by

$$\varrho_T \approx \frac{\log(\tilde{\eta}_T/\eta_T)}{\log(p_T/\tilde{p}_T)} + 1.$$

Here, the parameter ϱ_T may be interpreted as a measure for the local regularity. In that sense, the solution is sufficiently regular, if $\varrho_T \geq \max\{p_T, \tilde{p}_T\}$.

The first step of the hp -adaptive strategy is to compute η and to collect the mesh elements with the largest error contributions in a set $\mathcal{K} \subset \mathcal{T}$, for example, using one of the h -adaptive strategies described above. If the maximum rule above was used to determine the polynomial degrees for the edges in \mathcal{T} , then the second degree distribution \tilde{p} is determined by $\tilde{p}_T := p_T + 1$ for all $T \in \mathcal{K}$ and $\tilde{p}_T := p_T$ otherwise. For the minimum rule, another set \mathcal{L} containing all elements of \mathcal{T} adjacent to an element in \mathcal{K} via an edge is determined and the second degree distribution is given by $\tilde{p}_T := p_T + 1$ for all $T \in \mathcal{K} \cup \mathcal{L}$ to ensure the full local polynomial space on each element $T \in \mathcal{K}$. The next step is to compute a second finite element approximation along with some error estimator $\tilde{\eta}$ using the degree distribution \tilde{p} . In the last step, all elements with insufficient local regularity are refined, i.e., all $T \in \mathcal{K}$ with $\varrho_T < p_T + 1$, and the local polynomial degree is increased for all elements $T \in \mathcal{K}$ with $\varrho_T \geq p_T + 1$. In Figure 6, the steps of the hp -adaptive strategy are illustrated for the well-known L-shaped domain example with a singularity at the re-entrant corner, cf. Example 2.1.4 in [45].

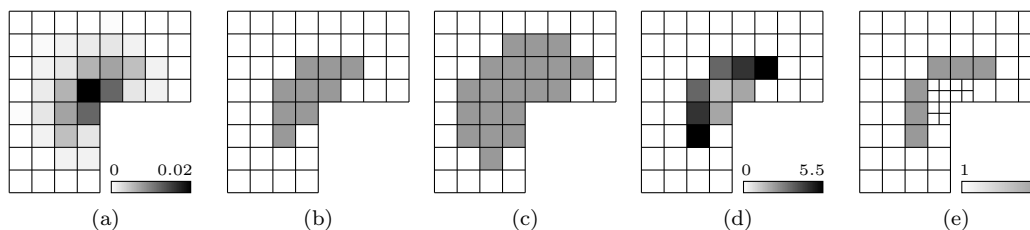


FIGURE 6. Visualization of the hp -adaptive refinement strategy: Error indicator η_T in (a), marked elements \mathcal{K} in (b), marked elements $\mathcal{K} \cup \mathcal{L}$ in (c), regularity indicator ϱ_T in (d) and the degree distribution p after the refinement in (e).

The computation of the additional error estimate $\tilde{\eta}$ obviously leads to high computational cost. However, this is justifiable by the exponential convergence rates of the adaptive scheme, see also Section 8. The proposed strategy is similar to the strategy proposed in [50], where the intermediate step to determine $\tilde{\eta}$ is omitted. Instead, only the first estimate η from two successive refinement steps are considered. However, error contributions of successive estimates are not necessarily comparable when using adaptive h -refinements and p -enrichments. Thus, those one-step strategies have to be applied carefully.

It is noted, that many h - and hp -adaptive strategies (including the strategy above) rely on the heuristic assumption, that the error contributions given by η_T reflect the local discretization error. Moreover, the increase of the local accuracy in areas with large error contributions is assumed to significantly reduce the global discretization error. These assumptions are well-justifiable in most cases and are confirmed by many numerical experiments. Though, convergence and, in particular, optimality are not guaranteed or theoretically verified in general. A rigorous verification of convergence and optimality of adaptive schemes is still an interesting field of research, see for instance [22, 23, 52]. For results concerning some hp -adaptive methods see also [34].

7.2. Error estimators. In this paper, a rather heuristic error estimator $\eta_T = |u_H - u_h|_{H^1(T)}$ based on a reference solution u_H is used for some of the numerical experiments in Section 8. This solution is obtained via a uniform mesh refinement ($h/2$) and a once uniformly increased polynomial degree distribution $p + 1$, see also [28, 38]. Given the higher-order XFEM based on the hierarchical shape functions discussed in Section 5, this estimator is straight forward

to implement and yields the desired results. However, the implied computational cost is non-neglectable compared to many other error estimators. Hence, this $h/2, p+1$ estimator may only serve as a proof of concept for the hp -adaptive XFEM. For recent results on error estimators for the XFEM, see for instance [19, 20, 37, 46, 58, 65].

7.3. Hanging nodes. Hanging nodes usually occur in the process of adaptive mesh refinement whenever one element is refined but at least one of its neighboring elements is not, see also Subsection 7.1. If these hanging nodes are not eliminated from the mesh using sophisticated refinement strategies, they have to be taken care of in the construction of the partition of unity and the higher-order enrichment functions. For the latter case, there are basically two possibilities. First, special shape functions may be introduced on elements that have hanging nodes on at least one of their edges, cf. [44, 69]. Second, the used (standard) shape functions may be constrained to enforce continuity. The latter technique is frequently referred to as constraint approximation, cf. [31, 60]. The approaches proposed in [44] and [31, 60] have already been discussed and compared in [41] for first-order shape functions in the framework of the XFEM.

As constraint approximation is the technique of choice for the handling of hanging nodes in higher-order FEM, it is summarized here in all brevity. Consider the situation depicted in Figure 7(a). To ensure continuity of aggregated modes associated to hanging edges via

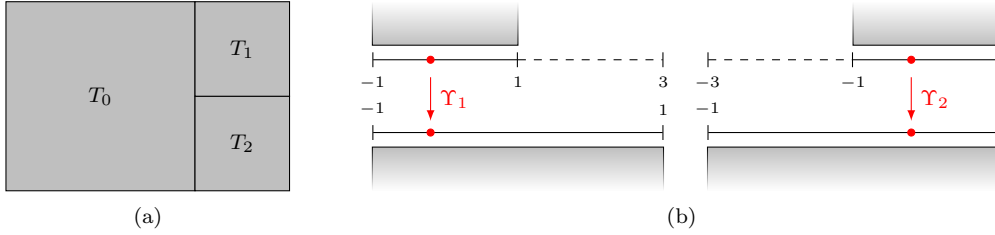


FIGURE 7. Mesh with a single hanging node (a). Visualization of Υ_k for the hanging edges resulting from the symmetric bisection via a hanging node (b).

constraint approximation, so-called constraints coefficients $\alpha_{i,j}^k \in \mathbb{R}$, $i, j \in I$ have to be found for the set of shape functions $\xi = \{\xi_i\}_{i \in I}$, such that

$$(29) \quad \xi_i \circ \Phi_{T_0}^{-1}(x) = \sum_{j \in I} \alpha_{i,j}^k \xi_j \circ \Phi_{T_k}^{-1}(x)$$

for all $x \in E_k = \overline{T_0} \cap \overline{T_k}$, $k \in \{1, 2\}$ and all $i \in I$. Obviously, only shape functions $\xi_i \circ \Phi_{T_k}^{-1}$ are of interest in (29) that do not vanish on E_k . Given the definition of ξ via a tensor product of one dimensional shape functions $\{\hat{\xi}_i\}_{i \in \{0, \dots, p\}}$, it is sufficient to find coefficients $\hat{\alpha}_{i,j}^k \in \mathbb{R}$, $i, j \in \{0, \dots, p\}$ such that

$$(30) \quad \hat{\xi}_i \circ \Phi_{E_0}^{-1}(x) = \sum_{j=0}^p \hat{\alpha}_{i,j}^k \hat{\xi}_j \circ \Phi_{E_k}^{-1}(x)$$

for all $x \in E_k$, $k \in \{1, 2\}$, where $\Phi_{E_k} : [-1, 1] \rightarrow E_k$ is a bijective, affine linear mapping and $E_0 = E_1 \cup E_2$. Let $\Upsilon_k(x) := a_k x + b_k$ with $a_k, b_k \in \mathbb{R}$ satisfy $\Phi_{E_0}^{-1}(x) = \Upsilon_k \circ \Phi_{E_k}^{-1}(x)$ for all $x \in E_k$, $k \in \{1, 2\}$. Hence, (30) is equivalent to

$$\hat{\xi}_i \circ \Upsilon_k(\hat{x}) = \sum_{j=0}^p \hat{\alpha}_{i,j}^k \hat{\xi}_j(\hat{x})$$

for $\hat{x} \in [-1, 1]$ and $k \in \{1, 2\}$. Let an edge be symmetrically bisected by a single hanging node. Thus, Υ_k can be defined as $\Upsilon_1(\hat{x}) := \frac{1}{2}(\hat{x} - 1)$, $\hat{x} \in [-1, 3]$ and $\Upsilon_2(\hat{x}) := \frac{1}{2}(\hat{x} + 1)$, $\hat{x} \in [-3, 1]$ as depicted in Figure 7(b).

Considering the set of Lagrange-type shape functions (12) along with their support points $\{\hat{x}^0, \dots, \hat{x}^p\}$, define functionals $\phi_j(v) := v(\hat{x}^j)$ for $j = 0, \dots, p$. Due to the Kronecker-delta property $\hat{\xi}_i(\hat{x}^j) = \delta_{ij}$, there holds $\hat{\alpha}_{i,j}^k = \phi_j(\hat{\xi}_i \circ \Upsilon_k) = (\hat{\xi}_i \circ \Upsilon_k)(\hat{x}^j)$. For the modified set of Lagrange-type shape functions (15) with $\phi_j(v)$ as above, this Kronecker-delta property is satisfied only for $i, j = 1, \dots, p-1$. Hence, there holds

$$\begin{aligned} \hat{\alpha}_{i,j}^k &= (\hat{\xi}_i \circ \Upsilon_k)(\hat{x}^j) && \text{for } i \in \{0, \dots, p\} \text{ and } j \in \{0, p\}, \\ \hat{\alpha}_{i,j}^k &= 0 && \text{for } i \in \{0, p\} \text{ and } j \in \{1, \dots, p-1\}, \\ \hat{\alpha}_{i,j}^k &= (\hat{\xi}_i \circ \Upsilon_k)(\hat{x}^j) - \hat{\alpha}_{i,0} \hat{\xi}_0(\hat{x}^j) - \hat{\alpha}_{i,p} \hat{\xi}_p(\hat{x}^j) && \text{for } i, j \in \{1, \dots, p-1\}. \end{aligned}$$

The functionals ϕ_j , $j = 0, \dots, p$ for the integrated Legendre and Gauss-Lobatto polynomials,

$$\phi_0(v) := v(-1), \quad \phi_1(v) := v(1), \quad \phi_j(v) := \frac{j(j-1)(2j-1)}{2\kappa_j^2} \int_{-1}^1 \frac{\hat{\xi}_j(x)v(x)}{\hat{\xi}_0(x)\hat{\xi}_1(x)} dx,$$

satisfy the Kronecker-delta property for $i = 2, \dots, p$ and $j = 0, \dots, p$. Similar to the modified set of Lagrange-type shape functions, there holds

$$\begin{aligned} \hat{\alpha}_{i,0}^k &= \hat{\xi}_i \circ \Upsilon_k(-1), \quad \hat{\alpha}_{i,1}^k = \hat{\xi}_i \circ \Upsilon_k(1) && \text{for } i \in \{0, \dots, p\}, \\ \hat{\alpha}_{i,j}^k &= 0 && \text{for } i \in \{0, 1\} \text{ and } j \in \{2, \dots, p\}, \\ \hat{\alpha}_{i,j}^k &= \phi_j(\hat{\xi}_i \circ \Upsilon_k) - \frac{2j-1}{2\kappa_j^2} ((-1)^j \hat{\alpha}_{i,0}^k + \hat{\alpha}_{i,1}^k) && \text{for } i, j \in \{2, \dots, p\}, \end{aligned}$$

since $\phi_j(\hat{\xi}_0) = (-1)^j (2j-1)/(2\kappa_j^2)$ and $\phi_j(\hat{\xi}_1) = (2j-1)/(2\kappa_j^2)$. Using suitable test points, a linear system of equations may be derived for the above to obtain the actual constraints coefficients without the integral representation implied by ϕ_i , see also [75]. However, it is noted that this method produces large numerical inaccuracies for high polynomial degrees. Alternatively, an explicit formula for $\hat{\alpha}_{i,j}^k$ without the integral representation is available that uses the recurrence relation (16) and admits a numerically stable evaluation, cf. [60].

Given the constraints coefficients above, it is possible to ensure continuity of the (standard) higher-order shape functions over edges containing hanging nodes. As a consequence, nodal modes associated to hanging nodes do not generate a self-contained partition of unity function, but contribute to the partition of unity functions associated to non-hanging nodes as depicted in Figure 8. Similarly, shape functions associated to hanging edges of a given constraining

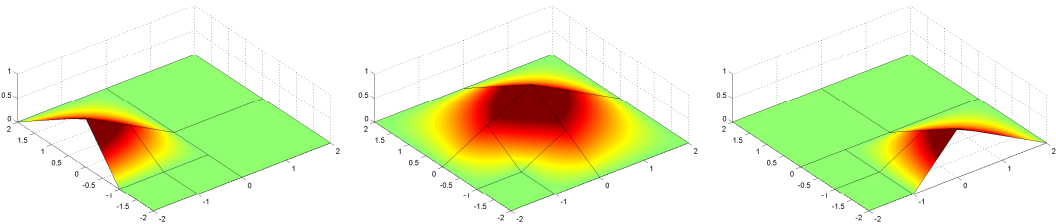


FIGURE 8. Visualization of the constrained bilinear partition of unity functions for a mesh with 2 hanging nodes.

edge do not define individual aggregated shape functions to be factorized, but contribute to the aggregation of shape function associated to that constraining edge. The factorization is then pursued via either adjacent constrained partition of unity function, as depicted in Figure 9. Obviously, the remainder resulting from the factorization of edge modes associated to constraining edges by either constrained partition of unity function is not necessarily a polynomial anymore.

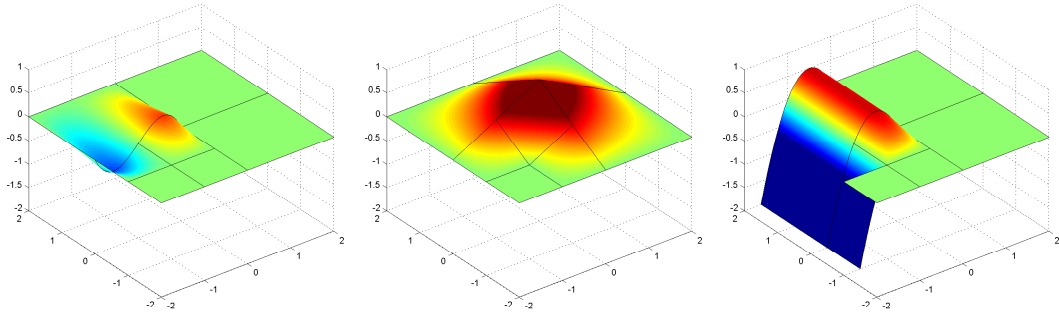


FIGURE 9. Visualization of the factorization of a constrained third-order hierarchical shape function associated to a constraining edge (left) into a constrained bilinear partition of unity function (middle) and some elementwise polynomial or rational function (right).

A discussion on the constraint approximation for the higher-order XFEM based on the hierarchical shape functions discussed in Section 5 with a focus on multi-hanging and unsymmetric hanging nodes will be pursued in a forthcoming paper.

7.4. Integration. As in standard finite element methods, the integrals in the discrete variational problem (3) are computed on the individual elements of decomposition \mathcal{T} of Ω and are added up. However, for the XFEM there arise two difficulties for the numerical integration.

The first difficulty is due to the discontinuous Heaviside enrichment. In the XFEM, cracks are allowed to be arbitrarily aligned in the domain under consideration. Hence, a crack path may intersect a given element of a mesh almost arbitrarily. Considering the usual crack propagation criteria, which provide an angle and some either predetermined or computed length for the crack propagation from the current crack tip, it is reasonable to assume that a crack Γ_C can be represented by a polygonal chain. Thus, Delauney-like sub-triangulations can be defined on each element $T \in \mathcal{T}$ cut by a crack, so that the edges of the sub-triangulation align with the polygonal chain of the crack path, cf. [16, 51, 17]. Hence, the usual Gauss quadrature of appropriate degree may be applied for the numerically exact integration of the crack path functions on each sub-element. Integration techniques that do not require sub-triangulations may for instance be found in [47, 54, 56, 71].

The second difficulty mentioned above is due to the crack tip functions which are in part discontinuous along the crack but also imply a $1/\sqrt{r}$ singularity for their derivatives at the crack tip. The discontinuity may for instance be handled with the sub-triangulations as above. To account for the singularity at the crack tip, the sub-triangulation of the element containing the crack tip may be chosen so that the crack tip is one of the vertices of each sub-element. Hence, a Duffy transformation may be used to concentrate the usual quadrilateral-based Gauss quadrature points towards the crack tip, cf. [36]. This integration technique, which is also referred to as the ‘almost polar integration’, yields improved integration properties, cf. [49]. A generalized Duffy transformation which can be adjusted to match the strength of the singularity is proposed in [53]. In [15], the integration of the crack tip functions is done via a transformation to a polar coordinate system, so that the $1/\sqrt{r}$ singularity of the derivatives of the crack tip functions (9) vanishes. The downside of the latter approach is that higher-order polynomials can no longer be integrated exactly.

7.5. Dirichlet boundary approximation. For higher-order finite element methods, it is of great importance to model inhomogeneous Dirichlet boundary conditions appropriately. Using the techniques proposed in [10], sufficiently regular inhomogeneous Dirichlet data can

be approximated with the accuracy required for the expected convergence rates of the higher-order finite element method.

8. NUMERICAL RESULTS

This section presents results obtained from the implementation of the higher-order XFEM based on integrated Legendre shape functions as proposed in Sections 3 and 5. The following numerical experiments for the model problem (1) for plane strain were carried out with Young's modulus $E = 10000$ and the Poisson ratio $\nu = 0.25$, as well as a fixed distance strategy for the crack tip enrichment with a radius $r = 1.0$. The ramp function technique as commemorated in Section 3 was not used to obtain the results below, except where explicitly noted.

A first benchmark problem is defined on a square domain $\Omega = [-2, 2]^2$ with the distribution of Dirichlet and Neumann boundary edges as depicted in Figure 10, where the sought displacement $u = (u_0, u_1)$ is a pure mode-I crack,

$$u_0(\theta, r) = \frac{1 + \nu}{2E} \sqrt{\frac{r}{2\pi}} K_I \left((5 - 8\nu) \cos \frac{\theta}{2} - \cos \frac{3\theta}{2} \right),$$

$$u_1(\theta, r) = \frac{1 + \nu}{2E} \sqrt{\frac{r}{2\pi}} K_I \left((7 - 8\nu) \sin \frac{\theta}{2} - \sin \frac{3\theta}{2} \right)$$

for polar coordinates (θ, r) of \mathbb{R}^2 .

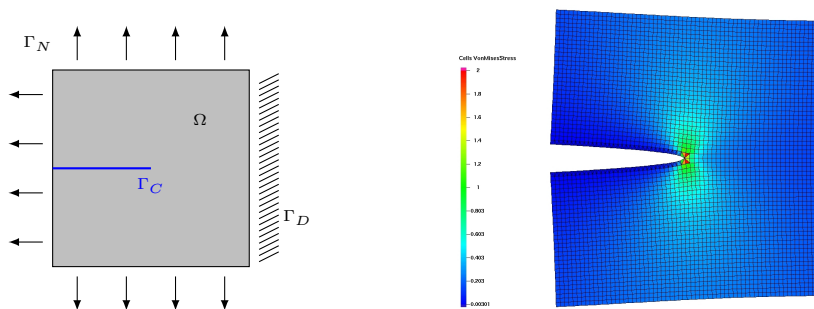


FIGURE 10. Domain $\Omega = [-2, 2]^2$ and boundary distribution (left). Von Mises stress and the scaled displacement for the first benchmark problem (right).

Figure 11 depicts the convergence history obtained for the first benchmark problem, using the h -version of the XFEM with fixed polynomial degrees $p = 1, \dots, 4$ and an uniform mesh refinement strategy. These methods exhibit optimal algebraic convergence rates even though no ramp function technique was used. Figure 12 illustrates the convergence rates obtained for the p -version of the XFEM with uniformly increasing polynomial degrees and for the hp -version of the XFEM, based on a fixed fraction criterion with $\theta = 0.2$ and $\eta_T = |u - u_h|_{H^1(T)}$. All methods exhibit exponential convergence rates. In particular, the error for either hp -XFEM is lower than that for the hp -FEM, where the crack is modeled through the doubling of edges. Furthermore, it is shown that the convergence rates for the hp -XFEM with and without the ramp function technique proposed in [39] are almost coincident. It is noted that the error indicator in the hp -adaptive XFEM only increased the polynomial degrees due to sufficient estimated regularity. Thus, there was no h -refinement pursued. To numerically verify the reliability and efficiency of the error estimator introduced in Subsection 7.2, the H^1 semi-error $|u - u_h|_{H^1(\Omega)}$ is depicted along with the $h/2, p + 1$ error estimator for uniform h -refinement in Figure 13. The convergence rates for the error and the estimated error are the same up to some constant for the individual polynomial degrees, respectively.

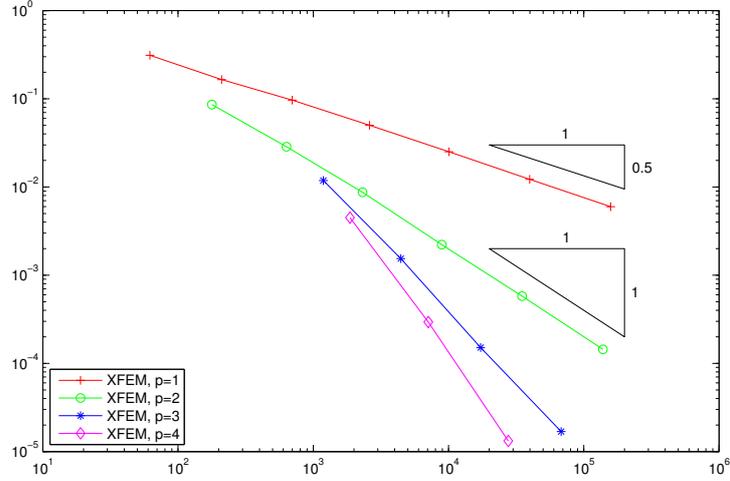


FIGURE 11. Convergence history: Degrees of freedom vs. H^1 semi-error $|u - u_h|_{H^1}$ for the h -version of the XFEM and uniform mesh refinement.

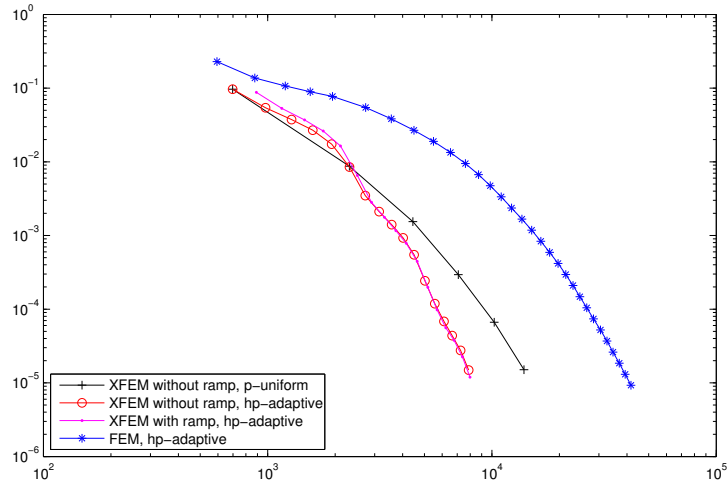


FIGURE 12. Convergence history: Degrees of freedom vs. H^1 semi-error $|u - u_h|_{H^1}$ for the p -uniform and the hp -adaptive version of the XFEM as well as the classic hp -adaptive FEM.

A second benchmark problem defined on $\Omega \subset (0, 5) \times (0, 4)$ is depicted in Figure 14, where a zero displacement $u_D = (0, 0)$ is imposed on Γ_D , a traction boundary condition $g = (0, 1)$ is imposed on Γ_{N_1} and a zero traction condition $g = (0, 0)$ is imposed anywhere else, i.e., on Γ_{N_0} and $\Gamma_C := [1, 2] \times \{2\}$.

In Figure 15, the convergence histories for the h -adaptive XFEM with $p = 1$ as well as the hp -adaptive XFEM and FEM are presented using the $h/2, p + 1$ error estimator introduced in Subsection 7.2. The h -adaptive XFEM with a bulk criterion and $\theta = 0.5$ exhibits an optimal algebraic convergence rate, where as both hp -methods with a fixed fraction criterion and $\theta = 0.2$ exhibit exponential convergence rates. However, the estimated error for the hp -XFEM

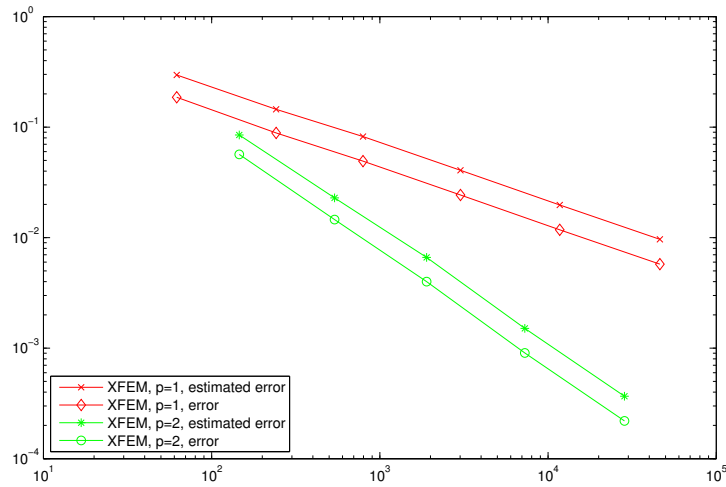


FIGURE 13. Convergence history: Degrees of freedom vs. H^1 semi-error $|u - u_h|_{H^1}$ and the $h/2, p+1$ estimated error as proposed in Subsection 7.2 for the h -version of the XFEM and uniform mesh refinement.

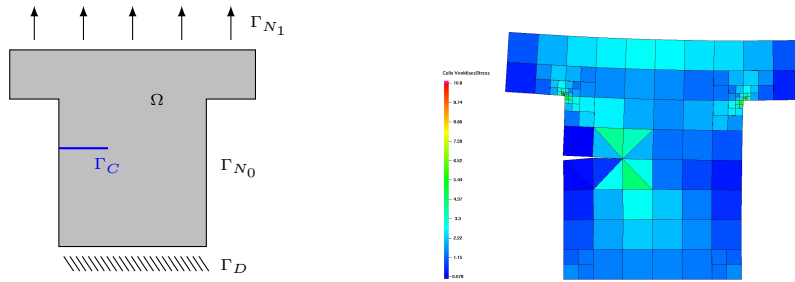


FIGURE 14. Domain Ω and the boundary distribution (left). Von Mises stress and the scaled displacement for the second benchmark problem (right).

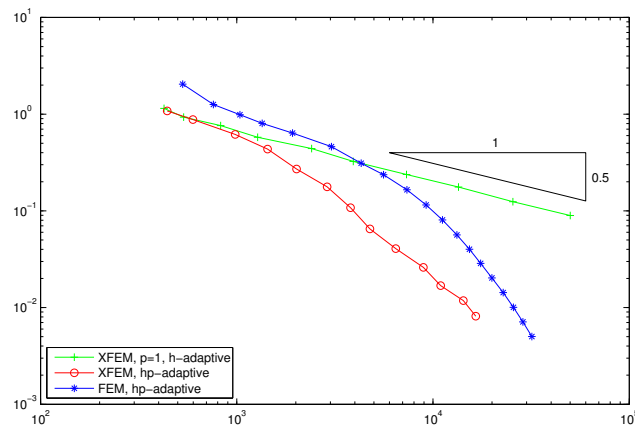


FIGURE 15. Convergence history: Degrees of Freedom vs. estimated error for the second benchmark problem.

is lower than that for the hp -FEM. The intermediate steps of the refinement for the hp -FEM and the hp -XFEM with similar numbers of degrees of freedom are depicted in Figures 16 and 17. As expected, the mesh for the hp -FEM exhibits strong mesh refinements towards the

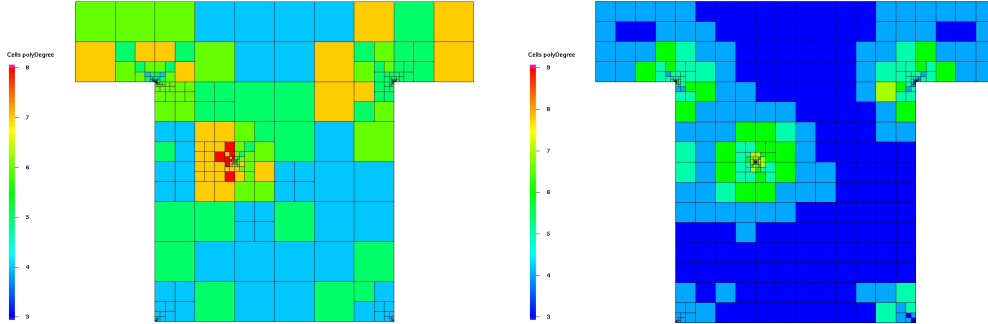


FIGURE 16. Visualization of the mesh and the polynomial degree distribution for an intermediate step of the hp -XFEM with 16530 degrees of freedom (left) and the hp -FEM with 17482 degrees of freedom (right).

reentrant corners as well as towards the crack tip. Similarly, the hp -XFEM also exhibits strong mesh refinements towards the reentrant corners as expected. However, there is also some slight refinement towards the crack tip. This refinement may be understood as the inability of the crack tip functions to model the crack tip displacement field exactly. However, compared to the refinement performed in the hp -FEM, this refinement is neglectable, see Figure 17.

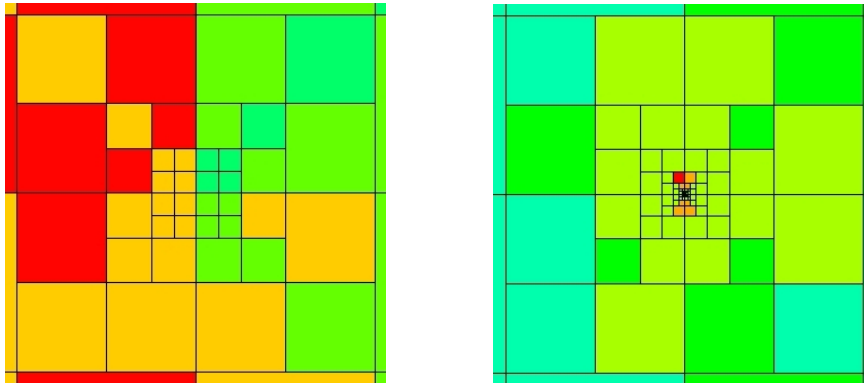


FIGURE 17. Zoom (10%) of the mesh at the crack tips for the hp -XFEM (left) and the hp -FEM (right).

The numerical results presented in this section, confirm the approximability results of the higher-order XFEM as discussed in Section 6. Furthermore, the superiority of the hp -method over the h -method as well as the superiority of the XFEM over the FEM in the framework of linear elastic fracture mechanics are confirmed.

9. CONCLUDING REMARKS

In this paper, a higher-order XFEM was obtained from the combination of the XFEM with standard higher-order FEM based on Lagrange-type and hierarchical tensor product shape functions. A priori error estimates were numerically verified for the standard mode I benchmark problem and optimal algebraic and exponential convergence rates were presented for a problem with reentrant corners. Furthermore, the methodological aspects necessary

for the presented numerical results were summarized. In particular, the handling of hanging nodes via constrained approximation and an *hp*-adaptive strategy were discussed. For future research, there remains a variety of challenges in the *hp*-adaptive XFEM:

- Apart from the well-known technical as well as modeling problems of the XFEM for three space dimensions, the extension of the proposed higher-order XFEM is straight forward due to the use of tensor-product shape functions.
- A discussion on the constraint approximation for the higher-order XFEM based on the hierarchical shape functions with a focus on multi-hanging as well as unsymmetric hanging nodes will be pursued in a forthcoming paper.
- The error estimator used in this paper is rather heuristic and computationally very expensive. An analysis of the applicability of well-established error estimators for the higher-order FEM as proposed in [2, 74] is part of our current research.
- The numerical experiments have pointed out that the crack tip functions spanning the Westergaard field are insufficient for problems, where the sought solution is not the Westergaard field itself. Hence, a generalization and an automatic adaptivity of these functions similar to the research presented in [76] is of great interest.

REFERENCES

1. Y. Abdelaziz and A. Hamouine, *A survey of the extended finite element*, Comp. Struc. **86** (2008), 1141–1151.
2. M. Ainsworth and J.T. Oden, *A posteriori error estimation in finite element analysis*, Wiley-Interscience, Chichester, 2000.
3. M. Ainsworth and B. Senior, *Aspects of an adaptive hp-finite element method: Adaptive strategy, conforming approximation and efficient solvers*, Comput. Methods Appl. Mech. Engrg. **150** (1997), 65–87.
4. D.N. Arnold, D. Boffi, and R.S. Falk, *Approximation by quadrilateral finite elements*, Math. Comput. **71** (2002), no. 239, 909–922.
5. I. Babuška, U. Banerjee, and J.E. Osborn, *Generalized finite element methods – main ideas, results and perspective*, Int. J. Comp. Meth. **1** (2004), 67–103.
6. I. Babuška and B.Q. Guo, *The h-p version of the finite element method with curved boundary*, SIAM J. Numer. Anal. **24** (1988), 837–861.
7. ———, *Regularity of the solution of elliptic problems with piecewise analytic data. part 1. boundary value problems for linear elliptic equation of second order*, SIAM J. Math. Anal. **19** (1988), no. 1, 172–203.
8. I. Babuška and J.M. Melenk, *The partition of unity method*, Int. J. Numer. Meth. Engrg. **40** (1997), 727–758.
9. I. Babuška and M. Suri, *The h-p version of the finite element method with quasi-uniform meshes*, Math. Mod. Numer. Anal. **21** (1987), 199–238.
10. ———, *The treatment of nonhomogeneous dirichlet boundary conditions by the p-version of the finite element method*, Numer. Math. **55** (1989), 97–121.
11. ———, *The p- and h-p versions of the finite element method, an overview*, Comput. Methods Appl. Mech. Engrg. **80** (1990), 5–26.
12. W. Bangerth and R. Rannacher, *Adaptive finite element methods for differential equations*, Birkhäuser, Basel, 2003.
13. F.B. Barros, S.P.B. Proença, and C.S. de Barcellos, *Generalized finite element method in structural non-linear analysis – a p-adaptive strategy*, Comput. Mech. **33** (2004), no. 2, 95–107.
14. ———, *On error estimator and p-adaptivity in the generalized finite element method.*, Int. J. Numer. Meth. Engrg. **60** (2004), no. 14, 2373–2398.
15. E. Béchet, H. Minnebo, N. Moës, and B. Burgardt, *Improved implementation and robustness study of the X-FEM for stress analysis around cracks*, Int. J. Numer. Meth. Engrg. **64** (2005), 1033–1056.
16. T. Belytschko and T. Black, *Elastic crack growth in finite elements with minimal remeshing*, Int. J. Numer. Meth. Engrg. **45** (1999), no. 5, 601–620.
17. T. Belytschko, N. Moës, S. Usui, and C. Parimi, *Arbitrary discontinuities in finite elements*, Int. J. Numer. Meth. Engrg. **50** (2001), 993–1013.
18. C. Bernardi and Y. Maday, *Spectral methods*, vol. 2, ch. 2, pp. 209–485, North-Holland, Amsterdam, 1997.
19. S. Bordas and M. Duflot, *Derivative recovery and a posteriori error estimate for extended finite elements*, Comput. Methods Appl. Mech. Engrg. **196** (2007), no. 35-36, 3381–3399. MR 2335273 (2008e:65325)
20. S. Bordas, M. Duflot, and P. Le, *A simple error estimator for extended finite elements*, Commun. Numer. Meth. Engrg. **24** (2008), 961 – 971.
21. É. Budyn, G. Zi, N. Moës, and T. Belytschko, *A method for multiple crack growth in brittle materials without remeshing*, Int. J. Numer. Meth. Engrg. **61** (2004), 1741–1770.

22. C. Carstensen, *Convergence of adaptive finite element methods in computational mechanics*, Appl. Numer. Math. **59** (2009), no. 9, 2119–2130.
23. C. Carstensen and C. Merdon, *Estimator competition for poisson problems*, J. Comput. Math. **28** (2010), no. 3, 309–330.
24. E. Chahine, P. Laborde, and Yves Renard, *Crack tip enrichment in the xfem using a cutoff function*, Int. J. Numer. Meth. Engng. **75** (2008), 629–646.
25. J. Chessa, H. Wang, and T. Belytschko, *On the construction of blending elements for local partition of unity enriched finite elements*, Int. J. Numer. Meth. Engng. **57** (2003), 1015–1038.
26. P.G. Ciarlet, *Mathematical elasticity. volume i: Three-dimensional elasticity*, North-Holland, Amsterdam, 1988.
27. L.F. Demkowicz, *Computing with hp-adaptive finite elements. vol. 1: One- and two-dimensional elliptic and maxwell problems. with cd-rom.*, Chapman & Hall/CRC Applied Mathematics and Nonlinear Science Series, 2007.
28. ———, *Polynomial exact sequences and projection-based interpolation with application to maxwell equations*, Mixed Finite Elements, Compatibility Conditions, and Applications, Lecture Notes in Mathematics, Springer Berlin / Heidelberg, 2008, pp. 101–158.
29. L.F. Demkowicz, K. Gerdes, C. Schwab, A. Bajer, and T. Walsh, *Hp90: A general and flexible fortran 90 hp-fe code*, Comput. Vis. Sci. **1** (1998), no. 3, 145–163.
30. L.F. Demkowicz, J. Kurtz, D. Pardo, M. Paszyński, W. Rachowicz, and A. Zdunek, *Computing with hp-adaptive finite elements. vol. ii: Frontiers: Three-dimensional elliptic and maxwell problems with applications.*, Chapman & Hall/CRC Applied Mathematics and Nonlinear Science Series, 2008.
31. L.F. Demkowicz, J.T. Oden, W. Rachowicz, and O. Hardy, *Toward a universal h-p adaptive finite element strategy. i: Constrained approximation and data structure.*, Comput. Methods Appl. Mech. Engrg. **77** (1989), no. 1-2, 79–112.
32. L.F. Demkowicz, W. Rachowicz, and P. Devloo, *A fully automatic hp-adaptivity*, J. Sci. Comput. **17** (2002), 117–142.
33. J. Dolbow, N. Moës, and T. Belytschko, *Discontinuous enrichment in finite elements with a partition of unity method*, Finite Elem. Anal. Des. **36** (2000), 235–260.
34. W. Dörfler and V. Heuveline, *Convergence of an adaptive hp finite element strategy in one space dimension*, Appl. Numer. Math. **57** (2007), no. 10, 1108–1124.
35. C.A. Duarte and J.T. Oden, *An h-p adaptive method using clouds*, Comp. Meth. Appl. Mech. Engrg. **139** (1996), 237–262.
36. M.G. Duffy, *Quadrature over a pyramid or cube of integrands with a singularity at a vertex*, SIAM J. Numer. Anal. **19** (1982), no. 6, 1260–1262.
37. M. Duflot and S. Bordas, *A posteriori error estimation for extended finite elements by an extended global recovery*, Int. J. Numer. Meth. Engng. **76** (2008), 1123–1138.
38. S. Ferraz-Leite, C. Ortner, and D. Praetorius, *Convergence of simple adaptive galerkin schemes based on h-h/2 error estimators*, Numer. Math. **116** (2010), 291–316.
39. T.-P. Fries, *A corrected xfem approximation without problems in blending elements*, Int. J. Numer. Meth. Engng. **75** (2008), 503–532.
40. T.-P. Fries and T. Belytschko, *The extended/generalized finite element method: An overview of the method and its applications*, Int. J. Numer. Meth. Engng. **84** (2010), no. 3, 253–304.
41. T.-P. Fries, A. Byfut, A. Alizada, K.W. Cheng, and A. Schröder, *Hanging nodes and xfem*, Int. J. Numer. Meth. Engng (2010).
42. B. Guo and I. Babuška, *The h-p version of the finite element method. part 1: The basic approximation results*, Comput. Mech. **1** (1986), no. 1, 21–41.
43. ———, *The h-p version of the finite element method. part 2: General results and applications*, Comput. Mech. **1** (1986), no. 3, 203–220.
44. A.K. Gupta, *A finite element for transition from a fine grid to a coarse grid*, Int. J. Numer. Meth. Engng. **12** (1978), 35–45.
45. W. Hackbusch, *Elliptic differential equations: Theory and numerical treatment*, Springer-Verlag, Berlin, 1992.
46. P. Hild, V. Lleras, and Y. Renard, *A posteriori error analysis for poisson's equation approximated by xfem*, ESAIM: Proc. **27** (2009), 107–121.
47. E.V. Iarve, *Mesh independent modelling of cracks by using higher order shape functions*, Int. J. Numer. Meth. Engng. **56** (2003), 869–882.
48. G.E. Karniadakis and S.J. Sherwin, *Spectral/hp element methods for cfd*, Oxford University Press, USA, 2005.
49. P. Laborde, J. Pommier, Y. Renard, and M. Salaün, *High-order extended finite element method for cracked domains*, Int. J. Numer. Meth. Engng. **64** (2005), 354–381.
50. J.M. Melenk and B.I. Wohlmuth, *On residual-based a posteriori error estimation in hp-fem*, Adv. Comput. Math. **15** (2001), no. 1-4, 311–331.

51. N. Moës, J. Dolbow, and T. Belytschko, *A finite element method for crack growth without remeshing*, Int. J. Numer. Meth. Engng. **46** (1999), no. 1, 131–150.
52. P. Morin, R.H. Nochetto, and K.G. Siebert, *Data oscillation and convergence of adaptive fem.*, SIAM J. Numer. Anal. **38** (2000), no. 2, 466–488.
53. S.E. Mousavi and N. Sukumar, *Generalized duffy transformation for integrating vertex singularities*, Comput. Mech. **45** (2010), no. 2-3, 127–140.
54. S. Natarajan, S. Bordas, and D.R. Mahapatra, *Numerical integration over arbitrary polygonal domains based on schwarz-christoffel conformal mapping*, Int. J. Numer. Meth. Engng. **80** (2009), no. 1, 103–134.
55. J.T. Oden, C.A. Duarte, and O.C. Zienkiewicz, *A new cloud-based hp finite element method*, Comp. Meth. Appl. Mech. Engrg. **139** (1996), 237–262.
56. M. Peters, *Modellierung von Rissausbreitung unter Verwendung der p-Version der XFEM mit einer adaptiven Integrationsmethode*, Ph.D. thesis, Ruhr-Universität Bochum, 2007.
57. W. Rachowicz, J.T. Oden, and L.F. Demkowicz, *Toward a universal h-p adaptive finite element strategy. iii: Design of h-p meshes*, Comp. Meth. Appl. Mech. Engrg. **77** (1989), no. 1-2, 181–212.
58. J.J. Ródenas, O.A. González-Estrada, J.E. Tarancón, and F.J. Fuenmayor, *A recovery-type error estimator for the extended finite element method based on singular+smooth stress field splitting*, Int. J. Numer. Meth. Engng. **76** (2008), 545–571.
59. A.M. Sanchez and R. Arcangeli, *Estimations des erreurs de meilleure approximation polynomiale et d'interpolation de lagrange dans les espaces de sobolev d'ordre non entier*, Numer. Math. **45** (1984), 301–321.
60. A. Schröder, *Constraints coefficients in hp - fem*, Numerical Mathematics and Advanced Applications, Springer Berlin Heidelberg, 2008, pp. 183–190.
61. C. Schwab, *p- and hp- finite element methods*, Numerical mathematics and scientific computing, Oxford University Press, 1998.
62. J.H. Song, H. Wang, and T. Belytschko, *A comparative study on finite element methods for dynamic fracture*, Comput. Mech. **42** (2008), no. 2, 239–250.
63. F.L. Stazi, E. Budyn, J. Chessa, and T. Belytschko, *An extended finite element method with higher-order elements for curved cracks*, Comput. Mech. **31** (2003), 38–48.
64. M. Stolarska, D.L. Chopp, N. Moës, and T. Belytschko, *Modelling crack growth by level sets in the extended finite element method*, Int. J. Numer. Meth. Engng. **51** (2001), 943–960.
65. T. Strouboulis, D. Wanga L. Zhanga, and I. Babuška, *A posteriori error estimation for generalized finite element methods*, Comp. Meth. Appl. Mech. Engrg. **195** (2006), no. 195, 852–879.
66. N. Sukumar, D.L. Chopp, N. Moës, and T. Belytschko, *Modeling holes and inclusions by level sets in the extended finite-element method*, Comput. Methods Appl. Mech. Engrg. **190** (2001), no. 46-47, 6183–6200. MR 1857695 (2002f:74077)
67. E. Süli, P. Houston, and C. Schwab, *hp-finite element methods for hyperbolic problems*, Tech. report, Oxford University Computing Laboratory, Parks Road, Oxford OX1 3QD, UK, 11 1999.
68. B. Szabó and I. Babuška, *Finite element analysis*, Wiley-Interscience. New York, John Wiley & Sons Ltd., 1991.
69. A. Tabarraei and N. Sukumar, *Extended finite element method on polygonal and quadtree meshes*, Comput. Methods Appl. Mech. Engrg. **197** (2008), 425–438.
70. J.E. Tarancón, A. Vercher, E. Giner, and F.J. Fuenmayor, *Enhanced blending elements for xfem applied to linear elastic fracture mechanics*, Int. J. Numer. Meth. Engng. **77** (2009), 126–148.
71. G. Ventura, *On the elimination of quadrature subcells for discontinuous functions in the eXtended Finite-Element Method*, Int. J. Numer. Meth. Engng. **66** (2006), no. 5, 761–795. MR 2219900 (2006k:74098)
72. G. Ventura, E. Budyn, and T. Belytschko, *Vector level sets for description of propagating cracks in finite elements*, Int. J. Numer. Meth. Engng. **58** (2003), 1571–1592.
73. G. Ventura, R. Gracie, and T. Belytschko, *Fast integration and weight function blending in the extended finite element method*, Int. J. Numer. Meth. Engng. **77** (2009), 1–29.
74. R. Verfürth, *A review of a posteriori error estimation and adaptive mesh-refinement techniques*, John Wiley & Sons, B. G. Teubner, Chichester, Stuttgart, 1996.
75. P. Šolín, K. Segeth, and I. Doležel, *Higher-order finite element methods*, Chapman & Hall/CRC Press, London/Boca Raton, 2003.
76. H. Waisman and T. Belytschko, *Parametric enrichment adaptivity by the extended finite element method*, Int. J. Numer. Meth. Engng. **73** (2008), no. 12, 1671–1692. MR 2397967

DEPARTMENT OF MATHEMATICS, HUMBOLDT UNIVERSITÄT ZU BERLIN, UNTER DEN LINDEN 6, D-10099 BERLIN, GERMANY

E-mail address: byfut@math.hu-berlin.de

DEPARTMENT OF MATHEMATICS, HUMBOLDT UNIVERSITÄT ZU BERLIN, UNTER DEN LINDEN 6, D-10099 BERLIN, GERMANY

E-mail address: schroder@math.hu-berlin.de